NANO LETTERS
Cite This: *Nano Lett.* 2019, 19, 1359−1365
Letter
pubs.acs.org/NanoLett

Effect of Net Charge on the Relative Stability of 2D Boron Allotropes

Dan Liu and David Tománek*

Physics and Astronomy Department, Michigan State University, East Lansing, Michigan 48824, United States

Supporting Information

ABSTRACT: We study the effect of electron doping on the bonding character and stability of two-dimensional (2D) structures of elemental boron, called borophene, which is known to form many stable allotropes. Our *ab initio* calculations for the neutral system reveal previously unknown stable 2D ϵ-B and ω-B structures. We find that the chemical bonding characteristic in this and other boron structures is strongly affected by extra charge. Beyond a critical degree of electron doping, the most stable allotrope changes from ϵ-B to a buckled honeycomb structure. Additional electron doping, mimicking a transformation of boron to carbon, causes a gradual decrease in the degree of buckling of the honeycomb lattice that can be interpreted as piezoelectric response. Net electron doping can be achieved by placing borophene in direct contact with layered electrides such as Ca_2N. We find that electron doping can be doubled by changing from the B/Ca_2N bilayer to the Ca_2N/B/Ca_2N sandwich geometry.

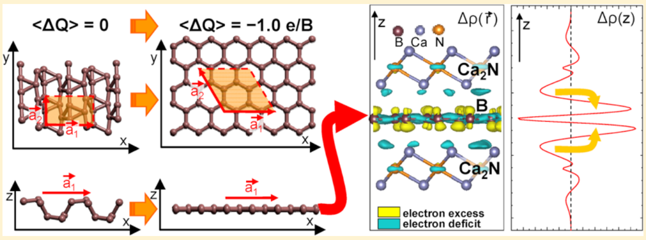

KEYWORDS: *Ab initio calculation, electronic structure, doping, boron, structural stability, 2D*

Identifying the most stable allotrope of a given compound is one of the key problems in physics and chemistry. Whereas charge-neutral systems have attracted the most attention, notable exceptions are low-dimensional systems that can be charged by doping in specific bulk geometries. Electron doping induced by Li intercalation does not affect the honeycomb structure of 2D graphene layers in graphite intercalation compounds (GICs)[1] but does change the equilibrium structure of MoS_2 monolayers from the 2H to the 1T allotrope.[2] Even though the effect of excess charge on chemical bonding and equilibrium geometry should be general, we expect the most drastic changes to occur in structures of elemental boron, which is notorious for its many stable allotropes.[3,4] What appears as frustrated bonding in mostly metallic 2D structures of elemental boron, called borophene, reflects the inability of the element to follow the octet rule of bonding due to its electron deficiency. We speculate that both the electron deficiency and thus the chemical bonding characteristic may be modified by placing a nonzero charge on B atoms. In that case, the most stable borophene structure may differ from a puckered triangular lattice with monatomic vacancies[5−9] or equally stable irregular structures[10−12] identified in the neutral system. Indeed, placing a net charge of $\lesssim 1$ e per atom on borophene, provided by an Al(111) substrate,[13] or intercalating Mg ions in between borophene layers in the MgB_2 compound,[14] changes the most stable allotrope to a very different honeycomb lattice. Structural changes induced by charging may significantly modify the electronic structure, turning semiconducting 2H-MoS_2 to metallic 1T′-MoS_2 locally[15] and undoped borophene to honeycomb lattices in diborides[16,17] including MgB_2, which displays superconducting behavior.[18]

In this study, we explore the effect of net charge on the bonding character and structural stability of 2D allotropes of boron. Our *ab initio* calculations for the neutral system reveal a previously unknown stable 2D ϵ-B structure with a 0.2 eV wide fundamental band gap. We find that the chemical bonding characteristic in this and other boron structures is strongly affected by extra charge, including a 23% lattice constant change in ϵ-B, induced by changing the net charge from 0.25 holes to 0.25 electrons per B atom. Beyond a critical degree of doping near 0.5 electrons/atom, the most stable allotrope changes from ϵ-B to a buckled honeycomb structure. Additional electron doping, mimicking a transformation of boron to carbon, causes a gradual decrease in the degree of buckling of the honeycomb lattice that can be interpreted as piezoelectric response. We propose that net electron doping can easily be achieved by placing borophene in direct contact with layered electrides such as Ca_2N. In this system, we find that electron doping of borophene can be doubled by changing from the B/Ca_2N bilayer to the Ca_2N/B/Ca_2N sandwich geometry.

As mentioned above, the vast number of stable neutral 2D borophene allotropes, including α-B, β-B, γ-B, δ-B, and η-B structures,[5,6] reflect a frustrated bonding character of electron-deficient boron. This element may engage its three valence electrons in only three covalent bonds, resulting in an electron sextet instead of the desirable octet noble-gas configuration. To partly compensate for the lack of electrons in the octet configuration, boron atoms often prefer to increase their coordination to six nearest neighbors in the triangular lattice.

Received: December 12, 2018
Revised: January 18, 2019
Published: January 23, 2019

ACS Publications © 2019 American Chemical Society

This is essentially equivalent to adding electrons[19,20] to the individual atoms that are held together by pure three-center bonding. On the contrary, the stability of the triangular lattice is often enhanced by removing atoms and forming hexagon-shaped monatomic vacancies. This process somehow mimics subtracting electrons while the structure locally converts to a honeycomb lattice, where atoms are held together by two-center bonding. The competition between two-center and three-center bonding has been used to identify the optimum concentration of hexagonal vacancies in the neutral triangular lattice[19,21,22] but likely also controls less common neutral structures with four- and five-fold coordinated boron atoms.[10,11] Biasing this competition by net charge has been shown to affect the fraction of hexagonal vacancies in triangular borophene lattices.[23] Even though doping of B layers has been linked to the unexpected superconducting behavior of MgB_2 and found to be useful to modulate CO_2 capture,[24] no systematic attention has been paid to the possibility of deliberately changing the bonding and the equilibrium structure of boron by excess charge.

A viable possibility to significantly dope 2D structures of elemental boron by electrons is to place them in direct contact with electrides including Ca_2N[25,26] and Y_2C.[27] In these highly electronegative systems with a layered structure, regions of large electron density are found in between the layers. The charge density in this electron layer amounts to one electron per formula unit in Ca_2N and two electrons per formula unit in Y_2C. The possibility of exfoliation down to a monolayer[25] has been demonstrated in Ca_2N, so that assembly of various vertical heterostructures is possible.

Results. *Allotropes of Neutral and Doped Borophene.* Inspired by the honeycomb structure of the negatively doped boron sublattice found in diborides including MgB_2, we started our investigation of electron-doped borophene structures with the honeycomb lattice. To provide substantial configuration freedom for the lattice structure, we consider a superlattice with 32 atoms per unit cell and subject all atoms in the supercell to random distortion. To study the effect of doping on the equilibrium structure and the chemical nature of bonding, we changed the degree of doping gradually and optimized each system using the conjugate gradient (CG) optimization method.

Starting with no excess charge, we found the neutral honeycomb structure to be unstable and to convert to rather stable allotropes that have not been reported previously. The first allotrope, shown in Figure 1a and called ϵ-B, is only 7 meV/atom less stable than the most stable α'-B phase[3] and displays a very uncommon morphology with triangles and pentagons, quite distinct from the well-documented class of triangular lattices with vacancies. The structure shown in Figure 1b, which we call ω-B, has a very similar morphology to known allotropes containing triangles and hexagons only[5−8] but is 26 meV/atom less stable than α'-B. ϵ-B and ω-B add to the large number of known allotropes, and we expect many more to follow.

Both ϵ-B and ω-B are buckled. Still, we could locate a locally stable, flat counterpart of ω-B, which is 7 meV/atom less stable than ω-B. The cohesive energies of neutral borophene allotropes are compared in Table 1.

Next, we added extra 5, 10, 13, 16, 24, and 32 electrons to the 32-atom unit cell with an initial honeycomb arrangements and optimized the geometry. We found the optimum geometries not to depend on initial deformations imposed on the starting structure, which may not be reachable in molecular dynamics trajectories. The optimum boron structures labeled $\epsilon_1-\epsilon_6$ and their average doping levels, $\langle\Delta Q\rangle$, are displayed in Figure 2a−f. Optimum structures for different doping levels are discussed in the Supporting Information (SI). We find all of these structures to differ significantly from the neutral ϵ-B and ω-B structures in Figure 1, which have been optimized in the same way.

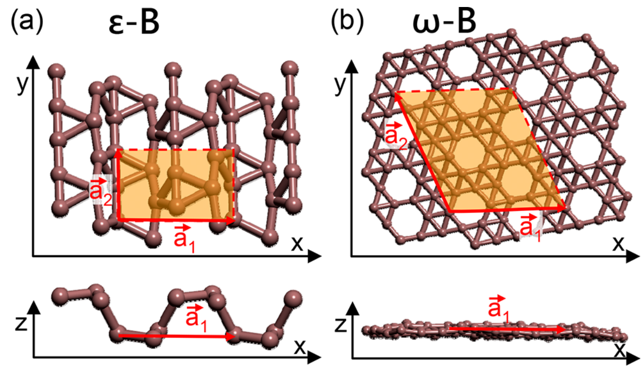

Figure 1. Previously unexplored neutral borophene allotropes formed by spontaneous conversion of an artificial honeycomb lattice: (a) ϵ-B and (b) ω-B. The structures are shown in top and side views. The lattice vectors $\vec{a}_1$ and $\vec{a}_2$, shown in red, delimiting the highlighted primitive unit cells.

Table 1. Cohesive Energy, E_{coh}, of Selected Neutral Borophene Allotropes, Obtained Using DFT-PBE Calculations[a]

allotrope	E_{coh} (eV/atom)	n	Z
ϵ-B	5.699[b]	8	4
ω-B	5.680[b]	32	4, 5, 6
α'-B	5.706[b]	8	5, 6
	5.762[c]	8	5, 6
β_{12}-B	5.712[c]	5	3, 5, 6
	6.23[d]	5	3, 5, 6
δ_6-B	5.662[c]	4	6
χ_3-B	5.723[c]	4	3, 5
	6.19[d]	4	3, 5

[a] n is the number of boron atoms per unit cell and Z is the coordination number of individual atoms in the unit cell. [b] Present work. [c] Ref 3. [d] Ref 8.

The structure ϵ_1-B in Figure 2a, which contains triangles, pentagons, and hexagons, is reminiscent of ϵ-B but is completely flat. With increasing electron doping, the density of pentagons gradually diminishes and eventually vanishes in ϵ_3-B in Figure 2c, representing the buckled χ_3 phase.[3] At the same time, the density of hexagons increases from ϵ_1-B to ϵ_3-B until all other polygons are eliminated in $\epsilon_4-\epsilon_6$, shown in Figure 2d−f, as the doping level exceeds $|\langle\Delta Q\rangle| \gtrsim 0.5$ e/atom. The buckled honeycomb lattice of ϵ_4-B gradually flattens to the graphene-like structure of ϵ_6-B with increasing electron doping.

The interpretation of these structural changes is rather straightforward. With one extra electron per atom, boron behaves as sp^2-bonded carbon with four valence electrons, with atoms forming the 2D graphene honeycomb lattice. This structure is rather robust with respect to electron and hole doping, as evidenced in GIC structures. Similarly, also, doped boron should keep its optimum honeycomb lattice structure even if the net charge may be smaller or larger than one extra

DOI: 10.1021/acs.nanolett.8b04968
Nano Lett. 2019, 19, 1359−1365

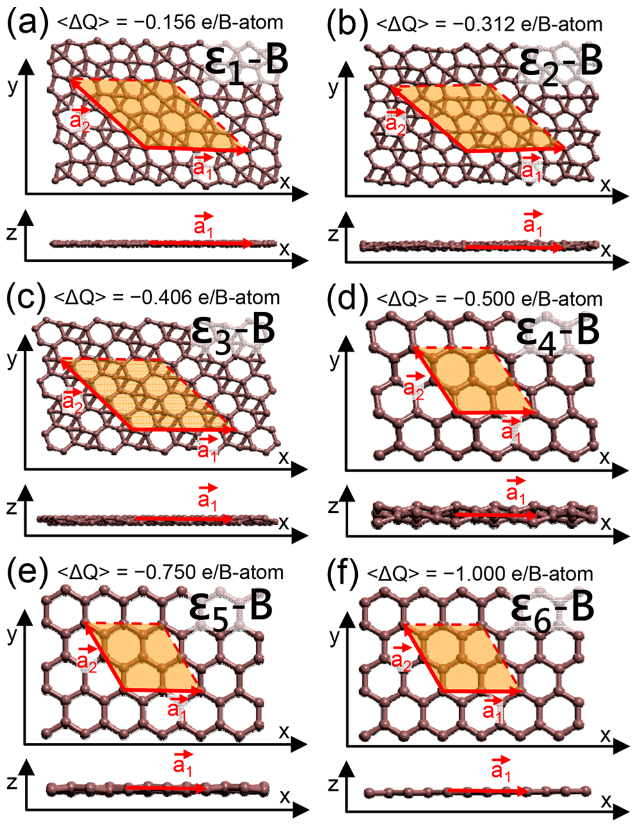

Figure 2. Electron-doped 2D borophene structures obtained by optimizing a distorted boron honeycomb superlattice with 32 atoms per unit cell. The average excess charge $\langle \Delta Q \rangle$ per boron atom, specified in the panels, increases from (a) ϵ_1-B to (f) ϵ_6-B. The structures are shown in top and side views. The lattice vectors $\vec{a}_1$ and $\vec{a}_2$, shown in red, delimit the highlighted unit cells.

electron per atom. As seen in Figure 2d−f, the honeycomb structure of borophene, with different degree of buckling, is preferred for the excess charge $\langle \Delta Q \rangle$ ranging between −0.5 and −1.0 e/atom.

To understand the change in the electronic structure that caused a profound structural change from neutral ϵ-B in Figure 1a to negatively charged ϵ_6-B^- in Figure 2f, we first probed the charge density changes, $\Delta\rho$, associated with charging. Our results for $\Delta\rho$ caused by placing artificially extra electrons on free-standing borophene structures ϵ_3-B and ϵ_6-B are shown in Figure 3a,b. $\Delta\rho$ can be viewed as the crystal counterpart of the Fukui function, and our results indicate that the extra electrons are accommodated in p_z (or π) states normal to the layer, very similar to graphene layers.

A realistic way to provide a high degree of electron doping, we suggest, is to place borophene layers in contact with the Ca_2N electride. The optimum lattice constant of the triangular lattice of Ca_2N is a = 3.97 Å. This layered system has the nominal configuration $[Ca_2N]^+ \cdot\ e^-$, with layers of Ca_2N separated by layers of excess electrons, and can be exfoliated down to a monolayer chemically.[25] It is to be expected that borophene will be electron-doped when placed in the region of excess electrons outside a Ca_2N monolayer. Because we focus on general trends rather than minute details, we studied the charge redistribution using only two prototype structures of doped borophene, namely, ϵ_3-B at low- and ϵ_6-B at high-level doping, in contact with Ca_2N. To determine the degree of electron doping in borophene caused by a contact to Ca_2N, we inspected the charge redistribution when placing ϵ_3-B and ϵ_6-B on top of a Ca_2N monolayer or, as in a sandwich geometry, in between Ca_2N monolayers. The charge density differences caused by electron redistribution in the system are shown in Figure 3c−f. Additional results for ϵ_3-B and ϵ_6-B on top of a $[Ca_2N]_2$ bilayer are presented in the SI.

We should point out that incommensurate vertical heterostructures formed of doped borophene and Ca_2N layers cannot be represented accurately in a periodic structure used in our computational approach. In our calculation, we used the optimum interlayer distance d = 4.0 Å in agreement with our results in Figure 4a,b. We furthermore matched 1 × 3 ϵ_3-B supercells with 3 × 7 Ca_2N supercells in the ϵ_3-B/Ca_2N superstructure and primitive unit cells of ϵ_6-B with 3 × 3 supercells of Ca_2N in the ϵ_6-B/Ca_2N superstructure. The remaining lattice mismatch of ≲2% was accommodated by averaging the lattice constants of borophene and Ca_2N. Because of this minor lattice distortion, results presented in Figure 3c−f may differ to a small degree from the charge redistribution in an incommensurate structure. Comparing results for the bilayer in Figure 3c,d with those in the sandwich structure in Figure 3e,f, we see clearly that borophene receives twice the number of electrons in the sandwich in comparison with the bilayer structure. Specifically, $\langle \Delta Q \rangle$ in ϵ_3-B almost doubles from −0.16 e/atom in Figure 3c to −0.31 e/atom in Figure 3e. Similarly, $\langle \Delta Q \rangle$ in ϵ_6-B almost doubles from −0.21 e/atom in Figure 3d to −0.41 e/atom in Figure 3f.

We have evaluated the dependence of the total energy on the interlayer distance, d, in the Ca_2N/B/Ca_2N sandwich structure for the ϵ_3-B and ϵ_6-B allotropes and present our results in Figure 4a,b. In both structures, the optimum interlayer distance $d \approx 4.0$ Å.

There is a significant electron accumulation with a maximum at $d \approx 3$ Å outside a free-standing Ca_2N electride layer,[25] which is accommodated by an adjacent borophene layer. In this case, the net charge on the borophene layer may be changed by changing the interlayer distance, d. Our results for $\langle \Delta Q \rangle$ as a function of d are presented in Figure 4c for ϵ_3-B and in Figure 4d for ϵ_6-B sandwiched in between two Ca_2N layers. We find it interesting that $\langle \Delta Q \rangle$ decreases almost linearly with increasing interlayer distance.

At the equilibrium interlayer distance, we find $\langle \Delta Q \rangle \approx -0.31$ e/B atom in the system with ϵ_3-B and $\langle \Delta Q \rangle \approx -0.41$ e/B atom in the system with ϵ_6-B. The higher value of $\langle \Delta Q \rangle$ in ϵ_6-B is associated with the better ability of this structure to accept electrons.

It is well known that in GICs the net charge transferred from dopant atoms to the graphene layers changes the lattice constant. This change is relatively small, amounting to[28] $\Delta a/a \approx 0.8\%$ in KC_8 with $\langle \Delta Q \rangle \approx -0.125$ e/C atom. Our corresponding results for the effect of doping on the lattice constants in the stable ϵ-B allotrope are shown in Figure 5a. The lattice changes are anisotropic and larger than found in graphene. We find that electron doping expands the lattice more along the softer $\vec{a}_1$ direction than along the harder $\vec{a}_2$ direction. At the electron-doping levels $\langle \Delta Q \rangle \approx -0.3$ to −0.5 e/B atom discussed above for the Ca_2N/B/Ca_2N heterostructures, the lattice expansion exceeds 10%.

The in-layer stiffness of neutral and electron- and hole-doped ϵ-B is addressed in Figure 5b. We used the shorthand notation 0 for the neutral system, − for $\langle \Delta Q \rangle$ = −0.125 e/B, and + for $\langle \Delta Q \rangle$ = +0.125 e/B doping. Irrespective of doping, the energy change due to in-layer strain, σ, is much larger along

DOI: 10.1021/acs.nanolett.8b04968
Nano Lett. 2019, 19, 1359−1365

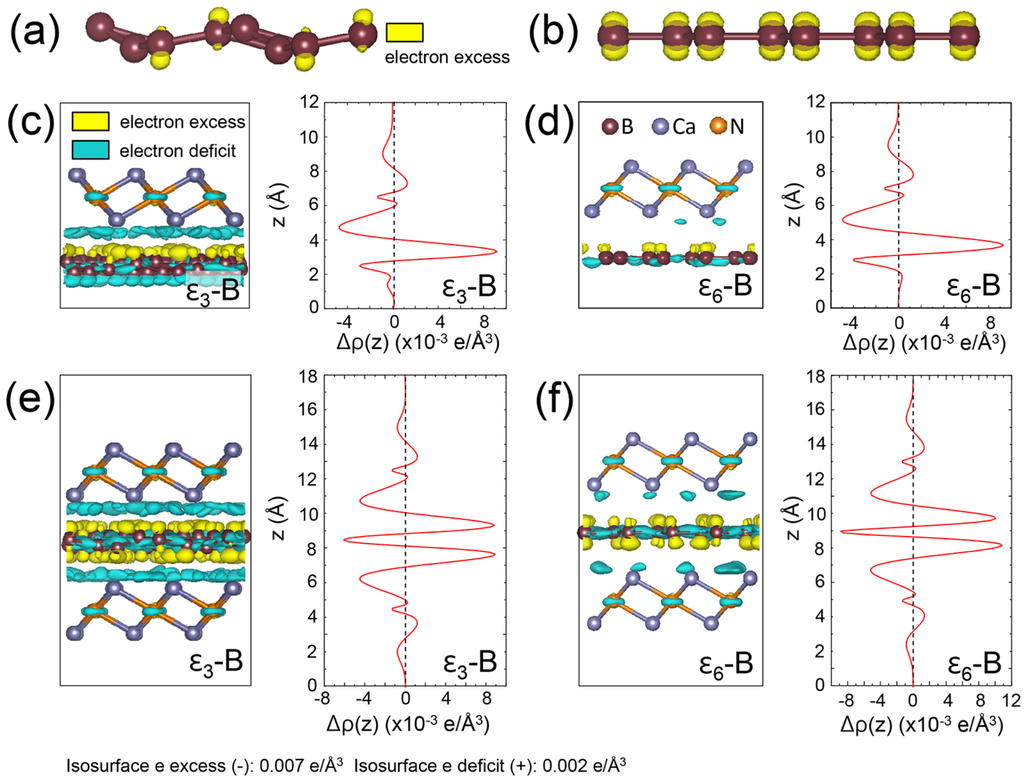

Figure 3. Charge redistribution in 2D borophene layers induced by electron doping or by contact with monolayers of Ca_2N electride. Charge density difference, $\Delta\rho$, caused by placing an excess charge (a) $\langle \Delta Q \rangle = -0.406$ e/atom on ϵ_3-B and (b) $\langle \Delta Q \rangle = -1.0$ e/atom on ϵ_6-B. Charge density redistribution $\Delta\rho = \rho(B/Ca_2N) - \rho(B) - \sum \rho(Ca_2N)$ in the bilayer structures (c) ϵ_3-B/Ca_2N and (d) ϵ_6-B/Ca_2N as well as in the sandwich structures (e) Ca_2N/ϵ_3-B/Ca_2N and (f) Ca_2N/ϵ_6-B/Ca_2N. $\Delta\rho$ is shown by isosurface bounding regions of electron excess at $+7 \times 10^{-3}$ e/Å^3 (yellow) and electron deficiency at -2×10^{-3} e/Å^3 (blue). $\langle \Delta\rho(z) \rangle$ is averaged across the $x-y$ plane of the layers.

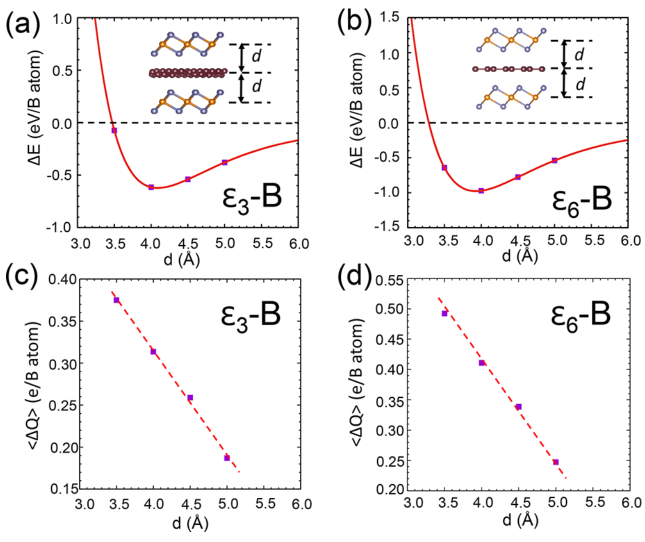

Figure 4. Changes in the interlayer interaction energy, ΔE, and net average charge, $\langle \Delta Q \rangle$, on borophene in the Ca_2N/B/Ca_2N sandwich geometry as a function of the interlayer distance, d. Results for ϵ_3-B in (a) and (c) are compared with those for ϵ_6-B in (b) and (d).

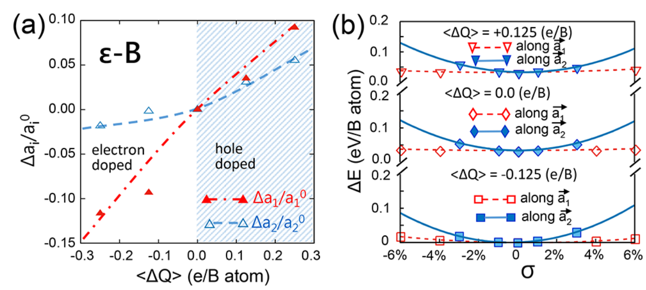

Figure 5. Effect of doping level on the equilibrium geometry of ϵ-B. (a) Effect of the net average charge, $\langle \Delta Q \rangle$, on the orthogonal lattice constants a_i with $i = 1,2$. Plotted are charge-induced relative changes $\Delta a_i/a_i^0$, where a_i^0 are the lattice constants in the neutral ϵ-B allotrope. (b) Strain energy, ΔE, as a function of in-layer strain, σ, at different doping levels, $\langle \Delta Q \rangle$.

the harder $\vec{a}_2$ direction than along the softer $\vec{a}_1$ direction. In terms of the 2D elastic constants,[29] we find for the softer $\vec{a}_1$ direction $c_{11}(-) = 67.99$ N/m, $c_{11}(0) = 18.70$ N/m, and $c_{11}(+) = 29.98$ N/m. Along the harder $\vec{a}_2$ direction, we find $c_{22}(-) = 446.79$ N/m, $c_{22}(0) = 360.52$ N/m, and $c_{22}(+) = 338.58$ N/m.

Electronic Structure of Borophene Allotropes. The electronic band structure of selected boron 2D allotropes discussed in this study is shown in Figure 6. We should note that density functional theory (DFT) calculations used in this study do not represent the true quasi-particle band structure and typically underestimate band gaps. With this fact in mind, we find that according to the Perdew−Burke−Ernzerhof (PBE) results in Figure 6a, the neutral ϵ-B allotrope of Figure 1a is a semiconductor with a small indirect band gap of $E_g = 0.2$ eV. Whereas stretching along the soft $\vec{a}_1$ direction by 4% turns ϵ-B into a direct-gap semiconductor, compressing by 4% along $\vec{a}_1$ causes gap closure. Stretching ϵ-B by 1% along the hard $\vec{a}_2$ direction turns this allotrope metallic, whereas compression by 1% changes its indirect gap to a direct gap. More details of the electronic structure of strained ϵ-B are provided in the SI.

DOI: 10.1021/acs.nanolett.8b04968
Nano Lett. 2019, 19, 1359−1365

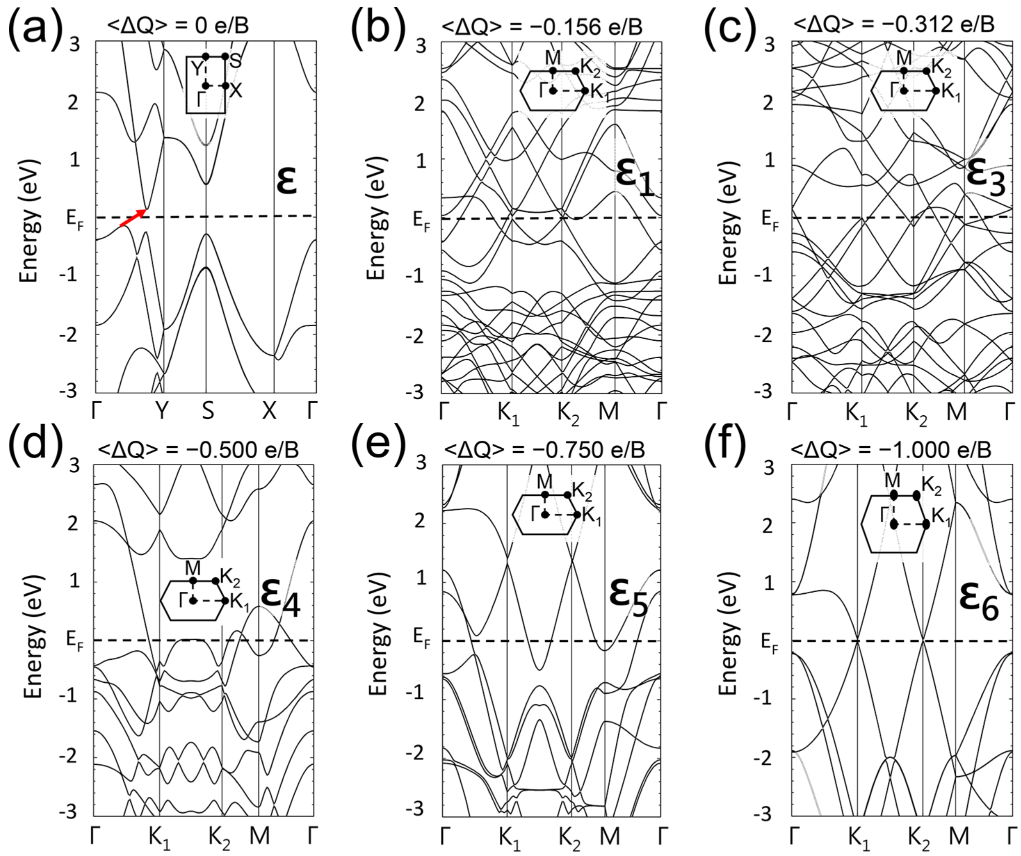

Figure 6. Electronic band structure of (a) neutral ϵ-B, (b) ϵ_1-B with $\langle \Delta Q \rangle = -0.156$ e/B, (c) ϵ_3-B with $\langle \Delta Q \rangle = -0.406$ e/B, (d) ϵ_4-B with $\langle \Delta Q \rangle = -0.500$ e/B, (e) ϵ_5-B with $\langle \Delta Q \rangle = -0.750$ e/B, and (f) ϵ_6-B with $\langle \Delta Q \rangle = -1.000$ e/B, calculated using the DFT-PBE functional. The indirect fundamental band gap is indicated by the red arrow in panel a.

We find all doped borophene allotropes to be metallic or semimetallic, as shown in Figure 6b−f. Inspection of the band structure reveals the formation of a Dirac cone at K_1 and K_2 in the honeycomb structures in ϵ_5-B in Figure 6e and in ϵ_6-B in Figure 6f. The Dirac cone appears ∼1.4 eV above E_F in ϵ_5-B at the doping level $\langle \Delta Q \rangle = -0.750$ e/B and at E_F in ϵ_6-B at $\langle \Delta Q \rangle = -1.000$ e/B, which mimics the structure and valence charge of graphitic carbon.

Discussion. The majority of the reported stable structures of neutral 2D borophene were triangular lattices containing arrays of monatomic vacancies, reflecting the frustrated bonding character of electron-deficient boron. When considering the effect of excess charge on the bonding geometry, we observed a transition driven by increasing net negative charge from structures containing triangles and higher polygons, depicted in Figures 1a and 2a−c, for $|\langle \Delta Q \rangle| < 0.5$ e/B to all-hexagon structures, depicted in Figure 2c−f, for $|\langle \Delta Q \rangle| > 0.5$ e/B. The highest coordinations number of six that may be achieved in a network of triangles reflects to some degree the vain attempt of neutral boron atoms to satisfy the octet rule. Excess negative charge, with the maximum value $|\langle \Delta Q \rangle| = 1.0$ e/B considered here, offers the ability to satisfy this rule in the honeycomb network of ϵ_6-B in Figure 2f.

To understand the chemical origin of these structural changes, we need to inspect the charge redistribution caused by additional doping, corresponding to the Fukui function for a crystal. Corresponding results for $\Delta\rho$ in selected electron-doped borophene structures are presented in the SI. Complementing our results presented in Figure 3 for borophene interacting with Ca_2N, these results suggest that additional electrons are first accommodated in p_z (or π) states normal to the borophene layer, which cause buckling, and then in σ states, which reduce the amount of buckling. Starting with the lightly electron-doped ϵ_1-B containing triangles, we observe an increasing degree of buckling with increasing electron doping up to $|\langle \Delta Q \rangle| \lesssim 0.5$ e/B. At that point, the structure changes to the honeycomb structure mimicking hole-doped graphene. For $|\langle \Delta Q \rangle| > 0.5$ e/B, additional excess charge gets increasingly accommodated in σ states, which are much closer to E_F in borophene than in graphene, causing a reduction of buckling down to zero for $\langle \Delta Q \rangle = -1.0$ e/B.

Assuming that the Ca_2N electride can transfer up to one electron per formula unit to a borophene layer, we can expect the maximum average charge $\langle \Delta Q \rangle$ per boron atom in B/Ca_2N bilayers to range from −0.22 e in ϵ_3-B/Ca_2N to −0.28 e/atom in ϵ_6-B/Ca_2N. The transferred charge may be up to twice as large in the Ca_2N/B/Ca_2N sandwich structures. These values are slightly larger but close to those found in the actual heterostructures, reported in Figure 3. We compared the charge transfer between monolayers and multilayers of the Ca_2N electride in contact with borophene and found essentially no difference, as seen in the SI. Thus the number of Ca_2N layers does not affect the maximum value of $\langle \Delta Q \rangle$.

It is not easy to achieve the doping level $\langle \Delta Q \rangle = -1.0$ e/B by contacting an electronegative material. According to our results for the Ca_2N/B/Ca_2N sandwich structure in Figure 4d, the Ca_2N electride can provide only up to ∼0.4 electrons per boron atom, much less than the desired doping level of 1 e/B.

DOI: 10.1021/acs.nanolett.8b04968
Nano Lett. 2019, 19, 1359−1365

An alternative to Ca_2N is Y_2C, which can supply twice as many electrons as Ca_2N but is hard to exfoliate. Assuming maximum charge transfer from Y_2C to borophene, B could receive up to 0.8 electrons in the $Y_2C/B/Y_2C$ heterostructure. Such a large electron transfer should further augment the Coulomb attraction between borophene and Y_2C, thus further deducing the interlayer distance, as seen in Figure 3a,b, and increase the amount of electron transfer, possibly up to 1.0 e/B.

We have mentioned electronic structure parallels between the honeycomb structure of ϵ_6-B carrying one extra electron per atom and graphene. Even though the system of π electrons near E_F and the Dirac cone in the corner of the Brillouin zone (BZ) occurs in both systems, there are notable differences between the systems. In graphene, the top of the σ band lies >3 eV below E_F, whereas this energy difference is only 0.2 eV in ϵ_6-B. Apparently, the lower core charge of elemental boron is the main reason why the σ and π bands are energetically closer than in graphene. As mentioned before, this results in an increased role of σ states in electron-doped borophene structures.

According to our results in Figure 5a, changing the doping level $\langle \Delta Q \rangle$ from −0.25 e to +0.25 e results in a 23% increase in the borophene lattice constant a_1. Conversely, we may speculate that changing the lattice constant should modulate the electron transfer from the electride to the borophene layer, thus changing the dipole moment normal to the interface. In that case, an in-plane vibration of the heterostructure will cause this dipole to oscillate and to emit an electromagnetic signal of the same frequency.

Clearly, the most drastic effect of electron doping is seen in the hexagonal borophene structure stabilized in MgB_2, which is the cause of superconductivity in this system. Electron doping may also be used as a way to change structures in a predictable way. As an illustration, we find the χ_3-B structure,[8] which has been synthesized at 680 K on Ag(111), to be very similar to the electron-doped, buckled ϵ_3-B structure. In that case, a simpler way to fabricate χ_3-B may consist of bringing borophene in contact with an electride, allowing it to relax to ϵ_3-B while electron-doped. The final flat structure of χ_3-B may evolve after the electride has been removed. These two examples illustrate new possibilities of using doping to change the structure of boron. Even though doping may have a lesser effect on the equilibrium structure of other systems, our findings about the interplay between structure and excess charge have a general validity.

In summary, we have studied the effect of electron doping on the bonding character and stability of 2D structures of elemental boron, called borophene, which is known to form many stable allotropes. Our *ab initio* calculations for the neutral system have revealed previously unknown stable 2D ϵ-B and ω-B structures in addition to previously reported triangular lattices with monatomic vacancies. We found that the chemical bonding characteristic in this and other boron structures is strongly affected by extra charge, which is first accommodated in the π and subsequently in the σ network of electrons. Beyond a critical degree of electron doping, the most stable allotrope was found to change from ϵ-B containing triangles and higher polygons to a buckled honeycomb structure. Additional electron doping, mimicking a transformation of boron to carbon, causes a gradual decrease in the degree of buckling of the honeycomb lattice that can be interpreted as a piezoelectric response. We also found that net electron doping can be achieved by placing borophene in direct contact with layered electrides such as Ca_2N. We found that electron doping can be doubled to ~0.4 e/B atom by changing from the B/Ca_2N bilayer to the $Ca_2N/B/Ca_2N$ sandwich geometry.

Computational Techniques. Our calculations of the stability, equilibrium structure, and electronic structure have been performed using DFT as implemented in the SIESTA[30] code. Periodic boundary conditions have been used throughout the study, with monolayers represented by a periodic array of slabs separated by a 30 Å thick vacuum region. We used the PBE[31] exchange-correlation functional. The SIESTA calculations used norm-conserving Troullier-Martins pseudopotentials,[32] a double-ζ basis including polarization orbitals, and a mesh cutoff energy of 250 Ry to determine the self-consistent charge density, which provided us with a precision in total energy of $\lesssim$2 meV/atom. The reciprocal space has been sampled by a fine grid[33] of 4 × 4 k-points in the 2D BZs of the primitive unit cells of neutral and doped borophene containing 32 atoms, 3 × 3 k-points in the BZ of supercell of heterostructure of Ca_2N and ϵ_6, and 3 × 1 k-points in the BZ of supercell of heterostructure of Ca_2N and ϵ_3. Geometries have been optimized using the CG method[34] until none of the residual Hellmann−Feynman forces exceeded 10^{-2} eV/Å.

■ ASSOCIATED CONTENT

Supporting Information

The Supporting Information is available free of charge on the ACS Publications website at DOI: 10.1021/acs.nanolett.8b04968.

Additional results are presented for the characterization of borophene layers under conditions not covered in the main manuscript. These include optimum geometries and charge distribution in free-standing electron-doped borophene as well as in vertical heterostructures of borophene and Ca_2N bilayers. Also presented are electronic band structures of systems described in the main manuscript, results characterizing the effect of strain on the electronic band structure, and charge density differences corresponding to the Fukui function for selected doped borophene allotropes (PDF)

■ AUTHOR INFORMATION

Corresponding Author

*E-mail: tomanek@pa.msu.edu.

ORCID

Dan Liu: 0000-0002-5211-4865

David Tománek: 0000-0003-1131-4788

Notes

The authors declare no competing financial interest.

■ ACKNOWLEDGMENTS

We acknowledge financial support by the NSF/AFOSR EFRI 2-DARE grant number EFMA-1433459. We thank Xianqing Lin, Andrii Kyrylchuk, and Rick Becker for many enriching discussions. Computational resources have been provided by the Michigan State University High Performance Computing Center.

■ REFERENCES

(1) Dresselhaus, M. S.; Dresselhaus, G. *Adv. Phys.* **1981**, *30*, 139−326.

(2) Py, M. A.; Haering, R. R. *Can. J. Phys.* **1983**, *61*, 76−84.

DOI: 10.1021/acs.nanolett.8b04968
Nano Lett. 2019, 19, 1359−1365

(3) Wu, X.; Dai, J.; Zhao, Y.; Zhuo, Z.; Yang, J.; Zeng, X. C. *ACS Nano* **2012**, *6*, 7443−7453.
(4) Quandt, A.; Boustani, I. *ChemPhysChem* **2005**, *6*, 2001−2008.
(5) Evans, M. H.; Joannopoulos, J. D.; Pantelides, S. T. *Phys. Rev. B: Condens. Matter Mater. Phys.* **2005**, *72*, 045434.
(6) Kunstmann, J.; Quandt, A. *Phys. Rev. B: Condens. Matter Mater. Phys.* **2006**, *74*, 035413.
(7) Mannix, A. J.; Zhou, X.-F.; Kiraly, B.; Wood, J. D.; Alducin, D.; Myers, B. D.; Liu, X.; Fisher, B. L.; Santiago, U.; Guest, J. R.; Yacaman, M. J.; Ponce, A.; Oganov, A. R.; Hersam, M. C.; Guisinger, N. P. *Science* **2015**, *350*, 1513−1516.
(8) Feng, B.; Zhang, J.; Zhong, Q.; Li, W.; Li, S.; Li, H.; Cheng, P.; Meng, S.; Chen, L.; Wu, K. *Nat. Chem.* **2016**, *8*, 563−568.
(9) Zhang, Z.; Penev, E. S.; Yakobson, B. I. *Chem. Soc. Rev.* **2017**, *46*, 6746−6763.
(10) Zhou, X.-F.; Dong, X.; Oganov, A. R.; Zhu, Q.; Tian, Y.; Wang, H.-T. *Phys. Rev. Lett.* **2014**, *112*, 085502.
(11) Zhou, X.-F.; Oganov, A. R.; Shao, X.; Zhu, Q.; Wang, H.-T. *Phys. Rev. Lett.* **2014**, *113*, 176101.
(12) Ma, F.; Jiao, Y.; Gao, G.; Gu, Y.; Bilic, A.; Chen, Z.; Du, A. *Nano Lett.* **2016**, *16*, 3022−3028.
(13) Li, W.; Kong, L.; Chen, C.; Gou, J.; Sheng, S.; Zhang, W.; Li, H.; Chen, L.; Cheng, P.; Wu, K. *Sci. Bull.* **2018**, *63*, 282−286.
(14) Nishibori, E.; Takata, M.; Sakata, M.; Tanaka, H.; Muranaka, T.; Akimitsu, J. *J. Phys. Soc. Jpn.* **2001**, *70*, 2252−2254.
(15) Kappera, R.; Voiry, D.; Yalcin, S. E.; Branch, B.; Gupta, G.; Mohite, A. D.; Chhowalla, M. *Nat. Mater.* **2014**, *13*, 1128.
(16) Perkins, P. G. In *Boron and Refractory Borides*; Matkovich, V., Ed.; Springer: Berlin, 1977; Chapter 3, pp 31−51.
(17) Kolmogorov, A. N.; Curtarolo, S. *Phys. Rev. B: Condens. Matter Mater. Phys.* **2006**, *74*, 224507.
(18) Nagamatsu, J.; Nakagawa, N.; Muranaka, T.; Zenitani, Y.; Akimitsu, J. *Nature* **2001**, *410*, 63−64.
(19) Tang, H.; Ismail-Beigi, S. *Phys. Rev. Lett.* **2007**, *99*, 115501.
(20) Tang, H.; Ismail-Beigi, S. *Phys. Rev. B: Condens. Matter Mater. Phys.* **2009**, *80*, 134113.
(21) Tang, H.; Ismail-Beigi, S. *Phys. Rev. B: Condens. Matter Mater. Phys.* **2010**, *82*, 115412.
(22) Karmodak, N.; Jemmis, E. D. *Angew. Chem., Int. Ed.* **2017**, *56*, 10093−10097.
(23) Tarkowski, T.; Majewski, J. A.; Gonzalez Szwacki, N. *FlatChem.* **2018**, *7*, 42−47.
(24) Tan, X.; Tahini, H. A.; Smith, S. C. *ACS Appl. Mater. Interfaces* **2017**, *9*, 19825−19830.
(25) Druffel, D. L.; Kuntz, K. L.; Woomer, A. H.; Alcorn, F. M.; Hu, J.; Donley, C. L.; Warren, S. C. *J. Am. Chem. Soc.* **2016**, *138*, 16089−16094.
(26) Lee, K.; Kim, S. W.; Toda, Y.; Matsuishi, S.; Hosono, H. *Nature* **2013**, *494*, 336−340.
(27) Zhang, X.; Xiao, Z.; Lei, H.; Toda, Y.; Matsuishi, S.; Kamiya, T.; Ueda, S.; Hosono, H. *Chem. Mater.* **2014**, *26*, 6638−6643.
(28) Nixon, D. E.; Parry, G. S. *J. Phys. C: Solid State Phys.* **1969**, *2*, 1732−1742.
(29) Liu, D.; Every, A. G.; Tománek, D. *Phys. Rev. B: Condens. Matter Mater. Phys.* **2016**, *94*, 165432.
(30) Artacho, E.; Anglada, E.; Dieguez, O.; Gale, J. D.; Garcia, A.; Junquera, J.; Martin, R. M.; Ordejon, P.; Pruneda, J. M.; Sanchez-Portal, D.; Soler, J. M. *J. Phys.: Condens. Matter* **2008**, *20*, 064208.
(31) Perdew, J. P.; Burke, K.; Ernzerhof, M. *Phys. Rev. Lett.* **1996**, *77*, 3865−3868.
(32) Troullier, N.; Martins, J. L. *Phys. Rev. B: Condens. Matter Mater. Phys.* **1991**, *43*, 1993−2006.
(33) Monkhorst, H. J.; Pack, J. D. *Phys. Rev. B* **1976**, *13*, 5188−5192.
(34) Hestenes, M. R.; Stiefel, E. J. *Res. Natl. Bur. Stand.* **1952**, *49*, 409−436.

DOI: 10.1021/acs.nanolett.8b04968
Nano Lett. 2019, 19, 1359−1365